DSC and Synchrotron-Radiation X-ray Diffraction Studies on Crystallization and Polymorphic Behavior of Palm Stearin in Bulk and Oil-in-Water Emulsion States

T. Sonoda[a,b], Y. Takata[a], S. Ueno[a], and K. Sato[a,*]

[a]Biomolecular Physical Chemistry Group, Graduate School of Biological Science, Hiroshima University, Higashi-Hiroshima, 739-8528, Japan, and [b]Pharmaceutical Development Laboratories, Tanabe Seiyaku Co., Ltd., Osaka, 532-8505, Japan

ABSTRACT: The crystallization and polymorphic behavior of palm stearin (PS) in a bulk state and in oil-in-water (O/W) emulsion droplets (average diameter, 1.7 ± 0.3 μm) was observed by using DSC, optical microscopy, and *in situ* X-ray diffraction with synchrotron radiation (SR-XRD). For the bulk sample, the DSC measurements revealed three main exothermic peaks at approximately 31 (large), 21 (small), and 3°C (medium) on cooling, and broad endothermic peaks at approximately –3 (small), 8, 15 to 25 (medium), and 37 and 53°C upon heating. The SR-XRD patterns taken during cooling from 60 to –5°C clarified that the DSC exothermic peaks around 31 and 3°C corresponded to crystallization of the α form of high-melting and low-melting fractions, respectively, and that the occurrence of β′ corresponded to the small exothermic peak around 21°C. The SR-XRD patterns taken during heating from –5 to 60°C demonstrated that the DSC endothermic peaks corresponded to the following transformation processes: melting of α of the low-melting fraction (–3°C), melt-mediated transformation from α to β′ (15–25°C), melting of β′ (36°C), and melting of β (53°C) of the high-melting fraction. As for the O/W emulsion sample, the DSC and SR-XRD measurements during the cooling and heating processes exhibited basically the same behavior as that of PS in the bulk state, except that β′ did not crystallize during the cooling process, and the temperatures of crystallization of α, melt-mediated $\alpha \rightarrow \beta' \rightarrow \beta$ transformation, and melting of β were lower in the emulsion droplets than in the bulk state.

Paper no. J10622 in *JAOCS 81,* 365–373 (April 2004).

KEY WORDS: Crystallization, DSC, emulsion, polymorphism, X-ray diffraction.

Fats and oils in an oil-in-water (O/W) emulsion state have been used in pharmaceuticals, foods, cosmetics, and agrochemicals. In pharmaceuticals, the O/W emulsion improves bioavailability for controlled release and sparingly water-soluble drugs (1,2). Thus far, O/W emulsion particles containing medium-chain FA TAG (MCT) and soybean oil have widely been used as drug carriers for injection (3). These emulsions do not crystallize at ambient temperatures, and drug materials can be solubilized owing to their high solubility in the emulsion droplets. When the oil phase of an emulsion is in a liquid state, however, the release of a loading drug from the emulsion is not readily controlled because of too high a rate of drug release (4). By contrast, when the oil phase in the emulsion contains high-melting fats, the rate of drug release can be modified since the rate of mass transfer of the drug materials incorporated in crystalline or semicrystalline phases is reduced compared with the liquid phase (4–6). Furthermore, polymorphic transformation of the fat crystals in an emulsion is also important, since drug release is modified by the crystal packing of the fats (7). Therefore, understanding the crystallization processes of fats in O/W emulsion droplets is of high interest in the manufacture of pharmaceuticals.

The main factors that affect fat crystallization properties in emulsion droplets are emulsion droplet size (8), emulsifiers (9), droplet–droplet interactions (9,10), additives present in the oil phase (11–14), and fat polymorphism and subsequent temperature history (15). Crystallization properties in emulsion have been summarized in recent reviews (16,17). To date, the crystallization properties in the emulsion state of mono-acid saturated TAG (18,19), cocoa butter (10), palm oil (20,21), palm midfraction (13), palm kernel oil (14), and milk fats (22,23) have been examined.

In this work, crystallization behavior and polymorphic transformation of palm stearin (PS) were examined in bulk and O/W emulsion states, with the ultimate aim of employing the micrometer- and nanometer-sized PS emulsion particles as drug carriers. For this purpose, the present work dealt with the crystallization and polymorphic properties of PS in the bulk and micrometer-sized emulsion states.

PS is obtained by fractionation of palm oil, which exhibits a wide range of melting temperatures (24,25). The polymorphic behavior of PS is remarkably complicated in comparison with simple TAG because PS contains different fat fractions with different melting, crystallization, and polymorphic transformation temperatures. Therefore, the polymorphism of PS is not fully understood, especially its kinetics in relation to polymorphism.

In the present experiments, we employed synchrotron radiation X-ray diffraction (SR-XRD) and DSC to analyze the rather complicated polymorphic properties of PS crystals. The SR-XRD measurements with small-angle scattering (SAXS) and

*To whom correspondence should be addressed at Graduate School of Biosphere Science, Hiroshima University, 1-4-4 Kagamiyama, Higashi-Hiroshima, 739-8528, Japan. E-mail: kyosato@hiroshima-u.ac.jp

wide-angle scattering (WAXS) analyses unveiled complicated polymorphic crystallization and transformation of PS in the bulk and emulsion states during cooling and heating processes, quite similarly to the fats exhibiting complicated transformation behavior reported previously (26–28). Conventional laboratory-scale X-ray diffraction techniques operating at lower rates of temperature variation cannot clarify the rapid and complicated polymorphic behavior of PS. The results obtained in the present work were discussed by taking into account our previous work on the mixing-phase behavior of PPP (tripalmitoyl-glycerol), POP (*sn*-1,3-dipalmitoyl-2-oleoylglycerol), PPO (1,2-dipalmitoyl-3-oleoylglycerol), and other TAG that make up PS (29–33), as well as recent studies of phase-transformation properties of monoacid TAG in nanometer-sized emulsion droplets (34,35).

MATERIALS AND METHODS

PS was provided by Fuji Oil Co., Ltd. (Osaka Japan); its FA composition and main TAG components are summarized in Table 1. Decaglycerin-monostearic acid ester (10G1S) with an HLB value of *ca.* 13.4 was provided by Sakamoto Pharmaceuticals Co., Ltd. (Osaka Japan) as an emulsifier for forming the O/W emulsion droplets. 10G1S is a food emulsifier from the group of polyglycerine FA esters that have polymerized glycerine molecules as a polar group and stearic acid as a hydrophobic chain. The average number of polymerized glycerine molecules is 10, and the degree of esterification is 1, so we refer to it as "10G1S" in this paper. The crystallization (melting) temperature of 10G1S was 44°C (46°C), as measured by DSC (data not shown).

O/W emulsion droplets were prepared by the method reported previously (12,14). Briefly, emulsification (20 wt% oil phase, 2 wt% emulsifier, and 78 wt% water phase) was performed in two stages. In the first stage, PS and distilled water with emulsifier 10G1S were mixed using a homogenizing mixer (pre-emulsification). In the second stage, final emulsification was performed by using a microfluidizer (8.5 kg/cm^3, four times) (Mizuho Industrial Co., Osaka, Japan). The average value of the particle diameter was measured using a laser particle-size analyzer (Model # SALD-2000J; Shimadzu, Kyoto, Japan) and calculated as 1.7 ± 0.3 μm.

The DSC experiments were carried out using a DSC-8230 (Rigaku, Tokyo, Japan). The sample was sealed in an aluminum pan, and Al_2O_3 was used as a reference material. The sample weighed 15 mg. The bulk sample was cooled from 60 to –10°C, maintained for 10 minutes at –10°C, then heated to 70°C. Different rates of cooling and heating were examined (1, 2, 5, and 10°C/min). The emulsion sample was cooled from 60 to –5°C, maintained for 10 min at –5°C, then heated to 60°C at the rates of 2 and 10°C/min. The two procedures yielded basically the same results. It was confirmed that the crystallization of PS in the droplets during the above cooling–reheating process did not cause serious particle coalescence, although partial coalescence was not avoided as revealed in a slight increase in an average droplet diameter measured at 40°C. It was also observed that all the particles showed total coalescence, when the emulsion particles were kept for several hours below 0°C. But this did not occur during the temperature variation described above.

TABLE 1
Chemical Analysis Data of Palm Stearin (%)

Composition of FA							
C12	C14	C16	C18	C18:1	C18:2	C18:3	C20
0.2	1.2	54.6	5.1	31.6	6.8	0.4	0.1

Composition of TAG (total number of carbon atoms of FA moieties)					
C46	C48	C50	C52	C54	C56
1.4	19.8	42.0	30.0	6.5	0.3

Time-resolved *in situ* small-angle and wide-angle X-ray scattering (SR-SAXS/WAXS) measurements using synchrotron radiation were performed with the synchrotron radiation source at the Photon Factory (beam line 15A) in the KEK Institute (Tsukuba, Japan). The methods of the SR-SAXS/WAXS experiments are fully described elsewhere (26). The temperature program of the SR-SAXS/WAXS began by heating from room temperature to 60°C, then cooling from 60 to –5°C, and finally heating from –5 to 60°C at a constant rate of 2°C/min. The sample, which weighed 24 mg, was placed in a $4 \times 4 \times 1.5$ mm^3 cell.

Fat crystallization of PS in the emulsion droplets was observed optically by putting the emulsion in a temperature-controlled growth cell (accuracy of temperature was ±0.1°C) and observing with polarized microscopy (magnification 40×) by cooling from 60 to 0°C. The method to prepare the emulsion droplets employed for the optical observation was the same as that explained above, except for the second-stage emulsification. The final emulsification was performed once by using the microfluidizer, so that the average diameter of the droplets was 2.5 μm, which could easily be observed with the optical microscope. To visualize both the oil droplets and the crystallized particles, we used two polarizers that were deviated slightly from a crossed Nichols position so that the crystallized droplets were brightened by birefringence of the PS crystals in the emulsion droplets.

RESULTS AND DISCUSSION

Bulk state. Figure 1 depicts the DSC cooling and heating thermopeaks of the PS bulk samples taken at different rates. The DSC peaks shown in Figure 1 were rescaled to account for the different cooling rates. Owing to the rather broad shape of the DSC exothermic and endothermic peaks, it was hard to determine the transformation temperatures with accuracy within 0.1°C. When the bulk sample was cooled, three main exothermic peaks were recorded: a main peak around 31°C, and medium peaks around 21 and 3°C. In contrast, multiple broad endothermic peaks appeared in a temperature range from –10 to 42°C, and a large peak appeared at 53°C in the heating process. Data taken at different cooling and heating rates were substantially the same, except for the peaks of crystallization at high temperature. Two peaks at 28 and 31°C, measured at a rate of 1°C/min, were combined into a single peak at rates of 2, 5, and 10°C/min. The temperature of the single exothermic peak decreased with increased cooling rates. It

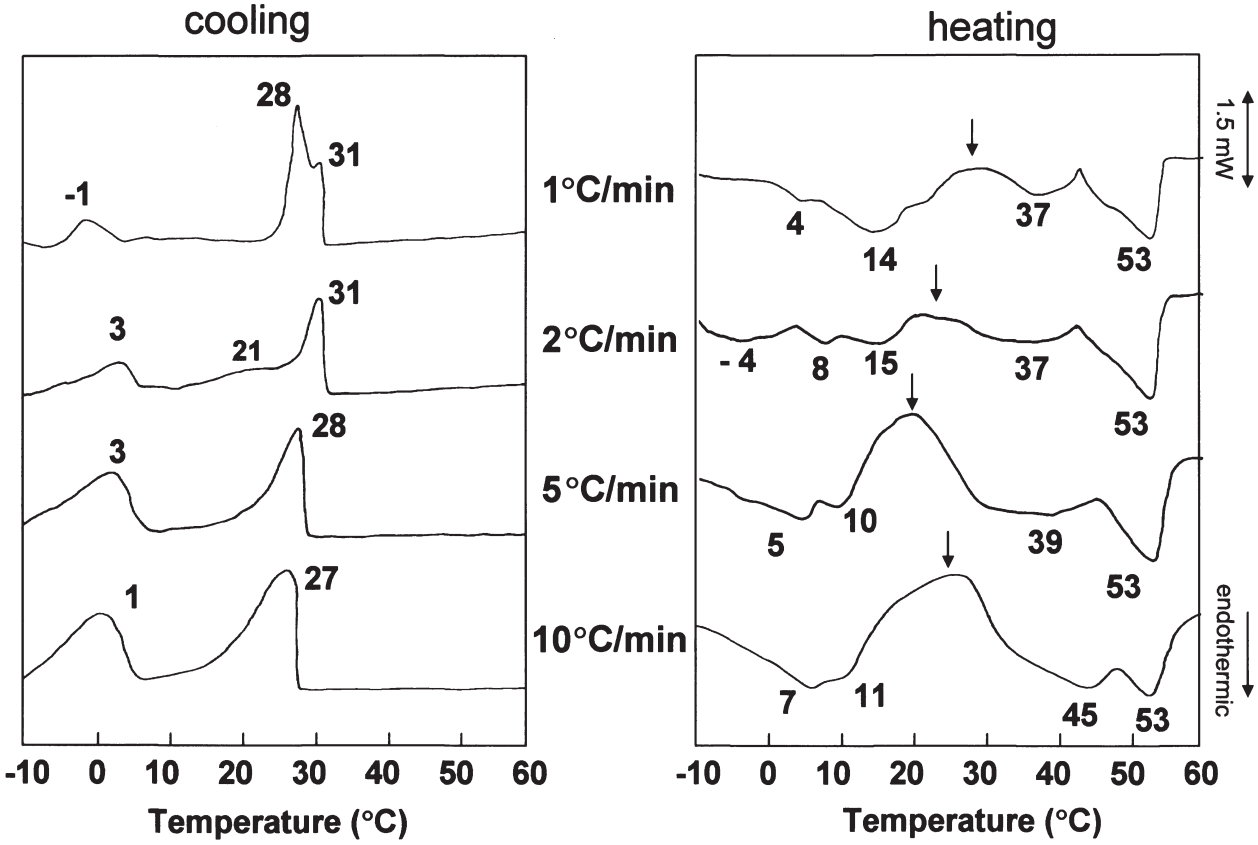

FIG. 1. DSC thermopeaks of bulk palm stearin at different rates of cooling and heating. Arrows in heating thermopeaks indicate melting of metastable forms and recrystallization of more stable forms of TAG fractions in palm stearin. The DSC peaks were rescaled to account for the different cooling rates.

is expected that melting of metastable forms, solid-state transformation, and recrystallization of more stable forms of low- and high-melting fractions of PS may complicate the DSC results during the heating process (in particular, for the peaks appearing in a temperature range from –10 to 42°C). These complexities could be resolved to some extent by the SR-XRD analysis.

Figure 2 presents SR-SAXS/WAXS data from the bulk sample of PS taken during the cooling (Fig. 2A) and heating (Fig. 2B) processes. An SR-SAXS pattern with a long-spacing (LS) value of 4.6 nm and an SR-WAXS pattern with a short spacing (SS) value of 0.42 nm appeared at 31°C, indicating the occurrence of the α form. On further cooling, another SAXS pattern with LS = 4.2 nm, a WAXS pattern with SS = 0.38 nm around 20°C, and SAXS patterns of 5.4 (001) and 2.7 nm (002) (which correspond to LS = 5.4 nm) appeared at 3°C. At this temperature, the intensity of the SAXS pattern of 0.42 nm increased. The SAXS (LS = 4.2 nm) and WAXS (SS = 0.38 and 0.43 nm) patterns corresponded to the β′ form. The same results were observed for the melting and crystallization processes of interesterified palm oil in an aerated emulsion system (21). The SAXS (LS = 5.4 nm) pattern corresponded to the α form because the corresponding WAXS pattern of SS = 0.42 nm increased its intensity at 3°C. This means that the DSC exothermic peak at 31°C observed during cooling is caused by crystallization of the α form, and another α form crystallized at 3°C when the exothermic peak appeared, as shown in Figure 1. The two α forms thus detected may be due to the presence of two fat fractions in PS with different crystallization temperatures. The small DSC exothermic peak at 21°C was caused by the crystallization of the β′ form of another fat fraction of PS. The crystallization of β′ with SS = 0.43 and 0.38 nm was also observed by SR-XRD in palm oil in aerated cream (21).

Figure 2B shows the SR-SAXS/WAXS data of the bulk sample taken during the heating process soon after the cooling process shown in Figure 3A. The melting of the α and β′ forms, the recrystallization of the β′ and β forms, and the melting of the β form are clearly shown in the WAXS patterns, and a complementary observation is presented in the SAXS patterns. The α form with LS = 5.4 nm disappeared around 3°C. The α form with LS = 4.6 nm then gradually decreased in its SAXS intensity upon heating from –5°C and sharply decreased at around 22°C. Correspondingly, the WAXS pattern of SS = 0.42 nm of the α form disappeared around 22°C. By contrast, the WAXS patterns of SS = 0.43 nm and of 0.38 nm of the β′ form, slightly increased in intensity around 35°C and disappeared around 45°C. As for the β′ form, it was difficult to describe the intensity changes with temperature upon heating because the SAXS pattern of the β′ form exhibited a shoulder pattern of the strong SAXS pattern of the α form (4.6 nm).

As a unique property of the heating data, the β form was crystallized and melted, although no β form was detectable during collection of the cooling data (Fig. 2A). The WAXS patterns of the β form with SS = 0.46, 0.39, and 0.37 nm started to appear around 35°C and disappeared around 53°C. Correspondingly, the SAXS pattern with LS = 4.2 nm appeared and disappeared at the same temperatures as those observed in the WAXS patterns. The appearance of the β form was caused by melt-mediated transformation from α and β′ during the heating process.

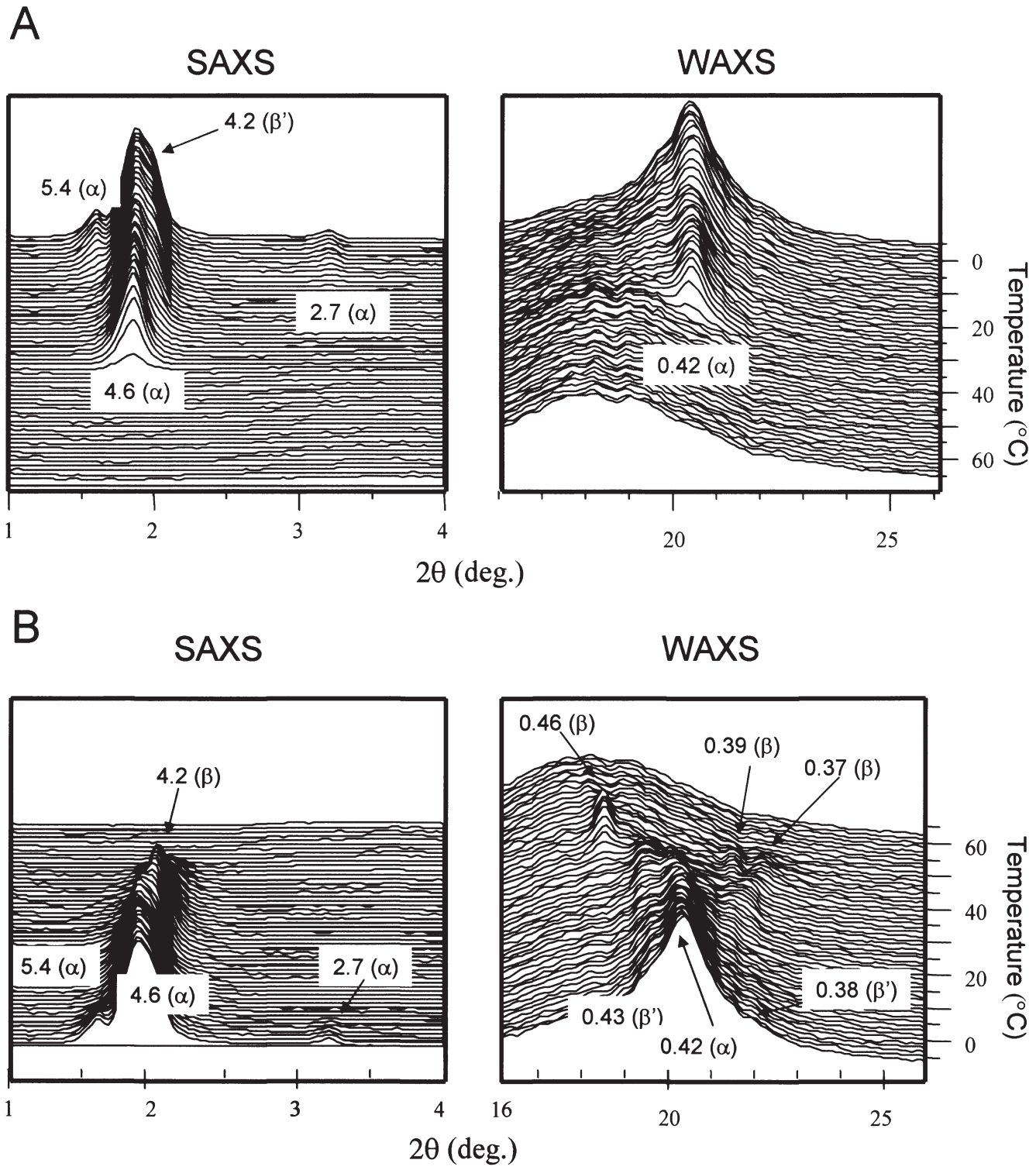

FIG. 2. Synchrotron-radiation (SR) X-ray diffraction long- and short-spacing patterns of palm stearin in a bulk state (A) during cooling from 60 to –5°C, and (B) during heating from –5 to 60°C after process A (unit: nm). SAXS, small-angle scattering; WAXS, wide-angle scattering.

Emulsion system. Figure 3 illustrates the DSC cooling and heating thermopeaks of PS in the emulsion sample. Compared with the bulk sample, the DSC peaks of the emulsion sample were broad and weak, particularly during the heating scan. Multiple exothermic peaks were detectable around 32, 27 and 3°C upon cooling. During heating, broad endothermic and exothermic peaks appeared in a temperature range of –5 to 42°C, and a large endothermic peak appeared around 51°C. The DSC cooling and heating peaks of the emulsion sample were more or less similar to those of the bulk sample, except for the absence of a broad exothermic peak around 20°C, and the lowered melting temperature of the high-melting fat fraction of PS (53°C in bulk and 51°C in emulsion, respectively). The polymorphic behavior indicated by DSC was examined by the SR-XRD experiments in more detail.

The panels of Figure 4 depict polarized optical micrographs of the emulsion droplets taken at 60, 30, and 0°C. By slightly deviating the angles of the two polarizers from the exact crossed Nichols position (90 degrees), it was possible to discern the oil droplets as dark images and crystallized droplets as bright images. At 60°C, all droplets were in a liquid state. At 30°C, several droplets appeared as bright images, presumably due to crystallization of high-melting fractions in the PS. At 0°C, many droplets became bright images. The optical micrographs in Figure 4 indicate that fat crystallization started from large-sized emulsion droplets at 30°C. The same features were recognized at 0°C. In a manner similar to crystallization in the emulsion droplets of *n*-alkane (36), we observed that coalescence of the emulsion droplets occurred after fat crystallization at 0°C. However, its detailed behavior was not fully examined in the present observation. In addition, very large particles with diameters of several tens of micrometers were observed, as shown in Figure 4. These large particles, however, did not correspond with those examined by DSC and XRD experiments, since the droplets shown in Figure 4 were prepared in a different manner from those examined by the other methods, as explained in a previous section.

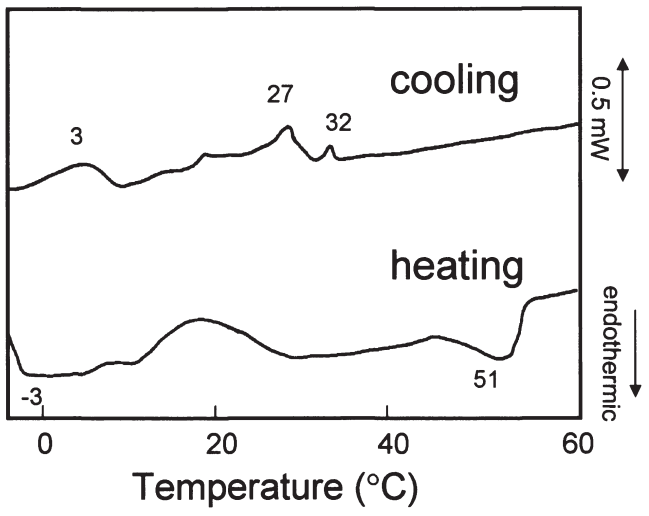

FIG. 3. DSC cooling and heating thermopeaks of a palm stearin emulsion.

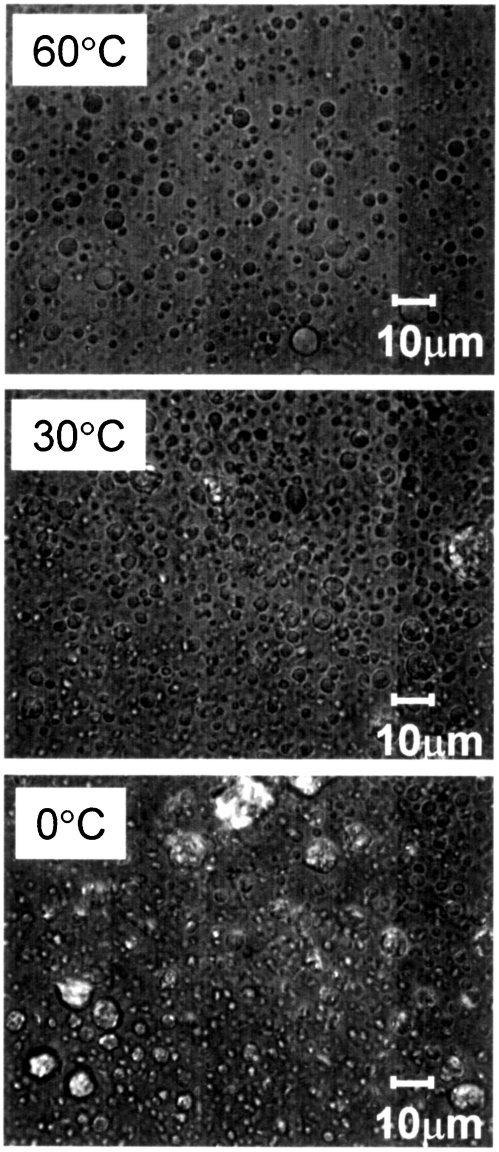

FIG. 4. Polarized optical micrographs of palm stearin emulsion droplets taken at different temperatures.

Figure 5 shows the SR-SAXS/WAXS data from the emulsion sample. The intensity of each diffraction pattern was lower than that of the bulk sample. During the cooling process (Fig. 5A), the SAXS/WAXS patterns exhibited the crystallization of the α form with LS = 4.6 nm and SS = 0.42 nm at 27°C. Upon further cooling, another α form with LS = 5.4 nm crystallized at 3°C. The crystallization of the β′ form was not detected, since no WAXS diffraction patterns of SS = 0.43 or 0.38 nm were observed. Figure 5B shows that upon heating, the α form with LS = 5.4 nm disappeared around 3°C, and the α form with LS = 4.6 nm disappeared around 25°C. Careful observation of the WAXS pattern showed that a weak pattern of the β′ form appeared around 15°C, then disappeared around 27°C. However, the corresponding SAXS pattern of the β′ form was not detectable. The β form started to appear around 18°C, as shown in the SAXS pattern. Weak WAXS patterns, together with noise

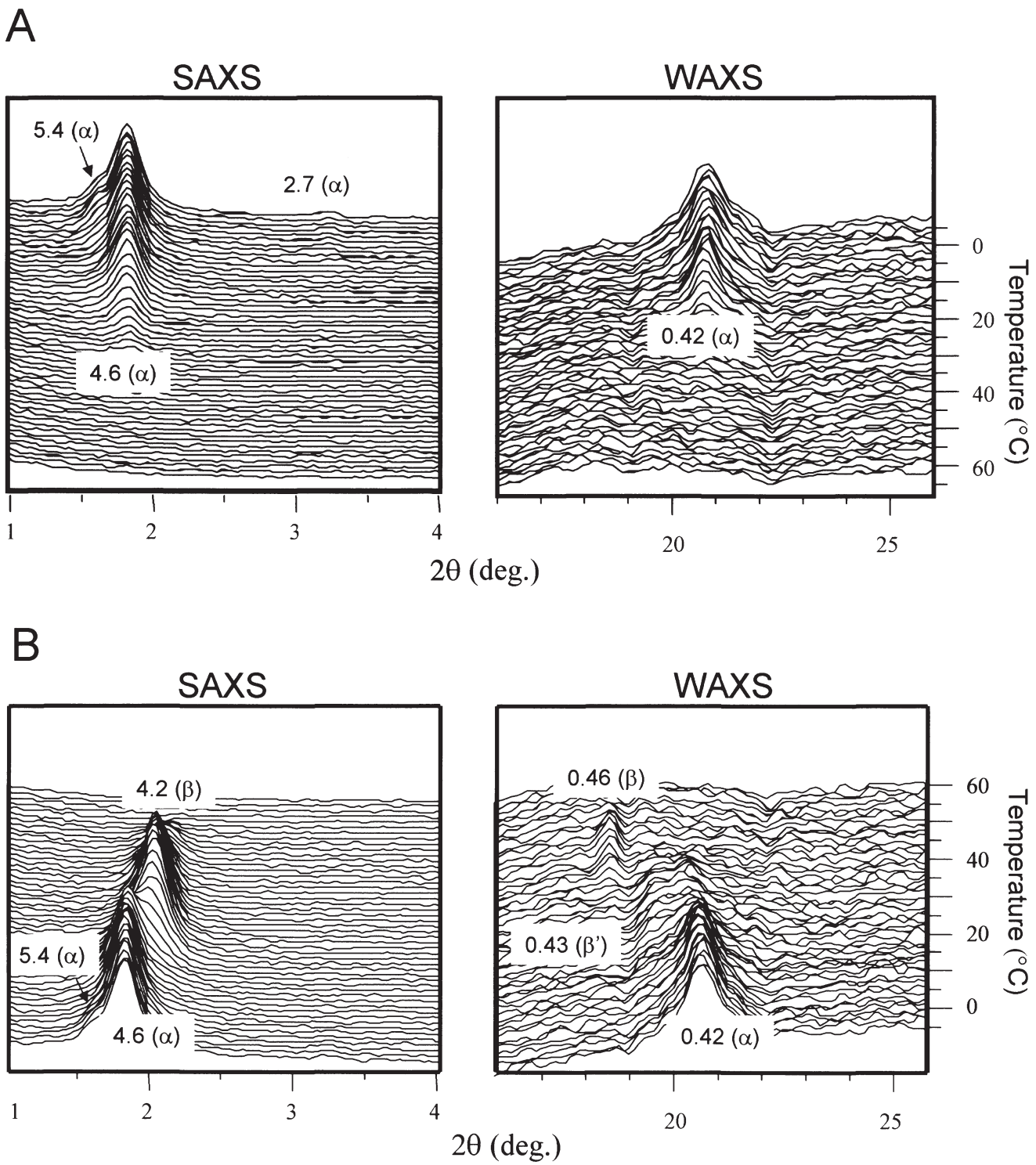

FIG. 5. SR-X-ray diffraction long- and short-spacing patterns of the palm stearin emulsion (A) during cooling from 60 to –5°C, and (B) during heating from –5 to 60°C (unit: nm). For abbreviations see Figure 2.

patterns, seemed to occur around 30°C, but we determined, as a result of its clarity, that the crystallization temperature of β was 18°C, in accordance with the SAXS pattern. The SAXS/WAXS patterns of the β form disappeared at 51°C during heating, indicating that the melting temperature of the β form of PS in emulsion was lower than that of the bulk sample (53°C).

Implications. PS is a fraction of palm oil separated by a dry fractionation method, and has the highest range of melting temperatures compared with other fractions (palm midfraction

and palm olein) (25). Even after the dry fractionation, PS contains multicomponent TAG. Therefore, as shown in Figure 1, the melting and crystallization temperatures are broadly distributed. In addition to the multiple TAG distribution, polymorphism also affects the complicated crystallization and melting behavior of PS. The present study using SR-XRD sought to clarify this complicated transformation behavior of PS.

Table 2 summarizes the correspondence of the experimental results of the DSC and SR-XRD measurements shown in Figures 1 and 2. SR-XRD patterns acquired during the heating process (Fig. 2A) revealed DSC peaks that were obviously quite complicated (Fig. 1). The large endothermic peak at 53°C was due to melting of the β form, whereas broad exothermic peaks around 14 to 30°C taken during heating (arrows in Fig. 1) corresponded to melting of the α form and the recrystallization of the β′ and β forms. Multiple endothermic peaks observed in a temperature range of –10 to 20°C during the cooling processes corresponded to the melting of the α forms of different fat fractions of PS. A broad endothermic peak around 37 to 45°C (Fig. 1 at different heating rates) was due to melting of the β′ form. Nearly the same feature of the crystallization and melting behavior of PS was observed in the emulsion state.

An interesting problem we encountered was how to characterize the multiple crystallization and melting behaviors of PS in terms of the phase behavior of every TAG component involved in PS. The major TAG components are PPP, POP (or PPO), 1-palmitoyl-2,3-dioleoyl glycerol (POO) (or OPO), and OOO (trioleoyl-glycerol), as judged from the composition of FA and TAG shown in Table 1. However, it seems that a full interpretation may not be straightforward, since the following systematic research must be performed in order to ascertain thorough answers to this question.

(*i*) *Analysis of TAG concentrations during each stage of crystallization.* As the cooling DSC thermopeaks indicate in Figure 1, there are at least two large fractions of TAG that exhibit unique crystallization and melting profiles through their cooperative interactions. For example, crystallization and melting occurring, respectively, around 31 and 53°C may be due to high-melting TAG fractions such as PPP, POP, or PPO. Furthermore, low-melting and crystallizing fractions such as POO (or OPO) and POL (or LOP) (1,3-palmitoyl-linoleoyl, 2-oleoyl-*rac*-glycerol) may cause crystallization and melting around the medium-temperature range.

(*ii*) *Analysis of phase behavior of the mixtures of TAG components.* This subject can be solved by examining the phase behavior of mixtures of component TAG for every fraction of PS. In doing so, one should bear in mind that binary mixtures of saturated–unsaturated mixed-acid TAG, such as POP, PPO and OPO, form molecular compound crystals (30–32), and those of PPP with POP show a eutectic mixture (29). In the former case, crystallization and polymorphic transformation occurred concurrently in the component TAG crystals and the molecular compound crystals of POP-PPO and POP-OPO, making the phase behavior quite complicated. For example, melting temperatures of the most stable forms are 31.2°C (β form of the compound), 35.2°C (β′ form of PPO), and 36.7°C (β form of POP) in the POP-PPO mixture (32). In the case of the eutectic mixture of PPP-POP, we found that the melting point of the β form of PPP decreased when the concentration of POP increased, e.g., 65°C (pure sample), 59°C (POP = 50 wt%), and 46°C (POP = 90 wt%) (29).

(*iii*) *Phase behavior of mixtures of different fractions of PS as related to the mixing behavior of high- and low-melting fractions.* This subject concerns the mixtures of the high-melting fat fractions containing PPP, POP, and PPO with liquid oil fractions of PS in which OOO (trioleoyl-glycerol) is assumed to be dominant.

Although the preceding three subjects are open to future work, we speculate that evidence for the TAG fractions of PS, whose major crystallization and melting behavior in the bulk state was shown in DSC and SR-XRD at the rate of 2°C/min, appears in the following: (i) PPP, POP, and PPO that crystallized around 27–31°C, (ii) POO or OPO that crystallized around 3°C, (iii) PPP (POP and PPO) that melted at 53°C (37°C), and (iv) the DSC heating thermopeaks around 10–43°C may involve α-melt-mediated transformation to β′ and β′-melt-mediated transformation to β in POP, PPO, or PPP.

The experimental results of DSC and SR-XRD studies of the O/W emulsion droplets are summarized in Table 2. The DSC exothermic and endothermic peaks correspond to the crystallization, melting, and melt-mediated transformation of the low- or high-melting fractions of PS in a manner similar to those of the bulk state, except for the small exothermic peak at 32°C. No detectable SR-XRD pattern was obtained at this temperature. We assume that this peak may be due to freezing of the FA chains of the emulsifier of 10G1S.

By comparing the melting features of the β form of the high-melting fraction of PS, we conclude that the temperatures of crystallization and melting of PS in the emulsion state

TABLE 2
Correspondence of DSC and SR-XRD Analyses measured at the Rate of 2°C/min

	DSC thermopeaks[a](°C)		SR-XRD analysis[b]
Bulk	Cooling	27–31 (L)	α (c)
		21 (S)	β′ (c)
		3 (M)	α (c)
	Heating	3 (M)	α (c)
		8–37 (M)	α (m)→ β′ (c), β′ (m)→ β (c)
		53 (L)	β (m)
Emulsion	Cooling	32 (S)	—
		15–27 (M)	α (c)
		3 (M)	α (c)
	Heating	–310 (M)	α (m)
		15–43 (M)	α (m)→ β′ (c), β′ (m)→ β (c)
		51 (L)	β (m)

[a]L, large peak; M, medium peak; S, small peak.
[b]c, crystallization; m, melting; SR-XRD, X-ray diffraction with synchrotron radiation.

are lower than those in the bulk state. The lower crystallization temperature in emulsion is consistent with those temperatures observed for *n*-alkane and fats in the emulsion (17). Povey (16) explained this effect as a reduced rate of heterogeneous nucleation of crystals in emulsion. However, the result of the lowered melting temperature is inconsistent with the fact that the melting temperature of *n*-hexadecane in the micrometer-sized O/W emulsion droplets did not differ from that in the bulk state (8,11). In contrast, it has been reported that the melting temperature is remarkably reduced in the nanometer-sized emulsion droplets of mono-acid TAG dispersed in a water phase (4,19,34,35). In these studies using droplets with diameters ranging from 30 to 200 nm, the degree of reduction in the m.p. ranged from several degrees Celsius (36) to about 20°C (4,19) depending on the average droplet diameters. It was evident that a smaller droplet diameter was associated with a higher degree of reduction in m.p. The main cause for the reduction in the m.p. is thought to be the increased chemical potential of small particles [Gibbs–Thomson effect (37)] and lattice defects (38). As for the present case of the micrometer-sized emulsion droplets, it may be assumed that the PS crystals formed in the droplet particles may contain large numbers of lattice defects, such as grain boundary and inhomogeneous blending of different TAG fractions, which reduced the melting temperature.

With regard to coalescence after fat crystallization, it was reported that the O/W emulsion using confectionery coating fat was destabilized by a cooling–heating thermocycling process (39). This instability was thought to be due to a partial coalescence mechanism by which crystallized particles interact during cooling and merge on melting. If this process occurs, DSC and XRD data after the coalescence have nothing to do with the properties of the emulsion state. In the present study, the emulsion sample was cooled from 60 to –5°C, maintained for 10 min at –5°C, and heated to 60°C at the rates of 2 and 10°C/min. We confirmed that the crystallization of PS in the droplets during the above cooling–reheating process did not cause any serious coalescence by observing that the emulsion sample exhibited a liquidus feature and that the size distribution did not change after the above temperature variation. Furthermore, we also observed that the same feature was confirmed when the emulsion sample was kept at 0°C for 24 h after this temperature variation. This result was reproducibly observed when we employed 10G1S as the emulsifier. However, when 10G1L (decaglycerine monolaurate), having a melting temperature lower than 10G1S, was employed as the emulsifier, total coalescence of the emulsion sample occurred very quickly at 0°C.

The different coalescence behavior due to the difference in the FA moieties of the polyglycerine esters may presumably be ascribed to interfacial crystallization (40). In the interfacial crystallization, the FA chains of the emulsifier and high-melting fraction in PS may cooperate to crystallize from the interfacial membrane of the emulsion droplets. It is expected that this phenomenon is similar to that caused by the addition of high-melting hydrophobic emulsifiers in the O/W emulsion droplets of *n*-alkane (11,12) and palm midfraction (13,14). We assume that the longer the FA chains, like 10G1S, the more the interfacial crystallization occurs. The interfacial crystallization might stabilize the emulsion particles more than the droplets without the interfacial crystallization, although the stabilization mechanism should be complicated.

ACKNOWLEDGMENTS

The authors wish to thank Prof. Yoshiyuki Amemiya, of the University of Tokyo, for cooperating in the preparation of the beam line BL-15A at the Photon Factory, in the KEK Institute (Tsukuba, Japan). The present work was partly supported by a Grant-in-Aid for Scientific Research (14540305), and by the Nano-Technology Project, Ministry of Agriculture, Forestry and Fisheries, Japan.

REFERENCES

1. Realdon, N., E. Ragazzi, M. Morpurgo, and E. Ragazzi, Influence of Processing Conditions in the Manufacture of O/W Creams: II. Effect on Drug Availability, *Farmaco 57*:349–353 (2002).
2. Kim, S.J., H. Choi, S. Suh, and Y. Lee, Pharmacokinetic and Pharmacodynamic Evaluation of Cyclosporin A O/W-Emulsion and Microsphere Formulations in Rabbits, *Eur. J. Pharm. Sci. 15:*497–502 (2002).
3. Wanten, G., J. Beunk, A. Naber, and D. Swinkels, Tocopherol Isoforms in Parenteral Lipid Emulsions and Neutrophil Activation, *Clin. Nutr. 21*:417–422 (2002).
4. Bunjes, H., B. Siekmann, and K. Westesen, Emulsions in Supercooled Melt—A Novel Drug Delivery System, in *Submicron Emulsions in Drug Targeting and Delivery,* edited by S. Benita, Harwood Academic Publishers, Singapore, 1998, pp. 175–204.
5. Dingler, H., R.P. Blum, H. Niehus, R.H. Muller, and S. Gohla, Solid Lipid Nanoparticles (SLN™/Lipopearls™)—A Pharmaceutical and Cosmetic Carrier for the Application of Vitamin E in Dermal Products, *J. Microencapsulation 16*:751–767 (1999).
6. Mehnert, W., and K. Mader, Solid Lipid Nanoparticles Production: Characterization and Applications, *Adv. Drug Del. Rev. 47*:165–196 (2001).
7. Jenning, V., M. Schafer-Korting, and S. Gohla, Vitamin A-Loaded Solid Lipid Nanoparticles for Topical Use: Drug Release Properties, *J. Controlled Rel. 66*:115–126 (2000).
8. Dickinson, E., D.J. McClements, and M.J.W. Povey, Ultrasonic Investigation of the Particle Size Dependence of Crystallization in *n*-Hexadecane–Water Emulsions, *J. Colloid Interface Sci. 142*:103–110 (1991).
9. McClements, D.J., E. Dickinson, S.R. Dungan, J.E. Kinsella, J.G. Ma, and M.W. Povey, Effect of Emulsifier Type on the Crystallization Kinetics of Oil-in-Water Emulsions Containing a Mixture of Solid and Liquid Droplets, *Ibid. 160*:293–297 (1993).
10. Hindle, S., M.J.W. Povey, and K. Smith, Kinetics of Crystallization in *n*-Hexadecane and Cocoa Butter Oil-in-Water Emulsions Accounting for Droplet Collision-Mediated Nucleation, *Ibid. 232*:370–380 (2000).
11. Kaneko, N., T. Horie, S. Ueno, J. Yano, T. Katsuragi, and K. Sato, Impurity Effects on Crystallization Rates of *n*-Hexadecane in Oil-in-Water Emulsions, *J. Crystal Growth 197*:263–270 (1999).
12. Katsuragi, T., N. Kaneko, and K. Sato, Effects of Addition of Hydrophobic Sucrose Fatty Acid Oligoesters on Crystallization Rates of *n*-Hexadecane in Oil-in-Water Emulsions, *Colloids Surf. B 20*:229–237 (2001).
13. Awad, T., and K. Sato, Effects of Hydrophobic Emulsifier Additives on Crystallization Behavior of Palm Mid Fraction in Oil-in-Water Emulsion, *J. Am. Oil Chem. Soc. 78*:837–842 (2001).

14. Awad, T., and K. Sato, Acceleration of Crystallization of Palm Kernel Oil in Oil-in-Water Emulsion by Hydrophobic Emulsifier Additives, *Colloids Surf. B 25*:45–53 (2002).
15. Coupland, J., E. Dickinson, D.J. McClements, M.J.W. Povey, and C.R. Mimmerand, Stability and Mechanical Properties, in *Food Colloids and Polymers,* edited by E. Dickinson and P. Walstra, Royal Society of Chemistry, Cambridge, 1993, pp. 243–249.
16. Povey, M.J.W., Crystallization of Oil-in-Water Emulsions, in *Crystallization Processes in Fats and Lipid Systems,* edited by N. Garti and K. Sato, Marcel Dekker, New York, 2001, pp. 251–288.
17. Coupland, J.N., Crystallization in Emulsions, *Curr. Opin. Coll. Interf. Sci. 7*:445–450 (2002).
18. Washington, C., and K. Evans, Release Rate Measurement of Model Hydrophobic Solutes from Submicron Triglyceride Emulsions, *J. Controlled Release 33*:383–390 (1995).
19. Bunjes, H., M.H.J. Koch, and K. Westesen, Effect of Particle Size on Colloidal Solid Triglycerides, *Langmuir 16*:5234–5241 (2000).
20. Hodate, Y., S. Ueno, J. Yano, T. Katsuragi, Y. Tesuka, T. Tagawa, N. Yoshimoto, and K. Sato, Ultrasonic Velocity Measurement of Crystallization Rate of Palm Oil in Oil-Water Emulsions, *Colloids Surf. A 128*:217–224 (1997).
21. Kalnin, D., G. Garnaud, A. Amentitsch, and M. Ollivon, Monitoring Fat Crystallization in Aerated Food Emulsions by Combined DSC and Time-Resolved Synchrotron X-ray Diffraction, *Rood Res. Intl. 35*:927–934 (2002).
22. Lopez, C., C. Bourgaux, P. Lesieur, S. Bernadou, G. Keller, and M. Ollivon, Thermal and Structural Behavior of Milk Fat: 3. Influence of Cooling Rate and Droplet Size on Cream Crystallization, *J. Colloid Interface Sci. 254*:64–78 (2002).
23. Lopez, C., P. Leieur, G. Keller, and M. Ollivon, Crystallization in Emulsion: Application to Thermal and Structural Behavior of Milk Fat, in *Crystallization and Solidification Properties of Lipids,* edited by N. Widlak, R.W. Hartel and S.S. Narine, AOCS Press, Champaign, 2001, pp. 190–199.
24. Basiron, Y., Edible Oil and Fat Products: Oils and Oilseeds, in *Bailey's Industrial Oil and Fat Products* 5th edn., edited by Y.H. Hui, John Wiley & Sons, New York, 1996, Vol. 2, pp. 217–345.
25. Smith, K.W., Crystallization of Palm Oil and Its Fractions, in *Crystallization of Oil-in-Water Emulsions,* edited by N. Garti, and K. Sato, Marcel Dekker, New York, 2001, pp. 357–380.
26. Ueno, S., A. Minato, H. Seto, Y. Amemiya, and K. Sato, Synchrotron Radiation X-ray Diffraction of Lipid Crystal Formation and Polymorphic Crystallization of SOS (*sn*-1,3-distearoyl-2-oleoyl glycerol), *J. Phys. Chem. B 101*:6847–6854 (1997).
27. Loisel, C., G. Keller, G. Lerg, C. Bourgaux, and M. Ollivon, Phase Transitions and Polymorphism of Cocoa Butter, *J. Am. Oil Chem. Soc. 75*:425–439 (1998).
28. Takeuchi, M., S. Ueno, E. Floeter, and K. Sato, Binary Phase Behavior of 1,3-Distearoyl-2-oleoyl-s*n*-glycerol (SOS) and 1,3-Distearoyl-2-lineoyl-*sn*-glycerol (SLS), *Ibid. 79*:627–632 (2002).
29. Minato, A., S. Ueno, J. Yano, Z.H. Wang, H. Seto, Y. Amemiya, and K. Sato, Synchrotron Radiation X-ray Diffraction Study on Phase Behavior of PPP-POP Binary Mixtures, *Ibid. 73*:1567–1572 (1996).
30. Minato, A., S. Ueno, J. Yano, K. Smith, H, Y. Amemiya, and K. Sato, Thermal and Structural Properties of *sn*-1,3-Dipalmitoyl-2-oleoylglycerol and *sn*-1,3-Oleoyl-2-palmitoylglycerol Binary Mixtures Examined with Synchrotron Radiation X-ray Diffraction, *Ibid. 74*:1213–1220 (1997).
31. Minato, M., J. Yano, S. Ueno, K. Smith, and K. Sato, FT-IR Study on Microscopic Structures and Conformations of POP-PPO and POP-OPO Molecular Compounds, *Chem. Phys. Lipids 88*:63–71 (1997).
32. Minato, M., S. Ueno, K. Smith, Y. Amemiya, and K. Sato, Thermodynamic and Kinetic Study on Phase Behavior of Binary Mixtures of POP and PPO Forming Molecular Compound Systems, *J. Phys. Chem. B 101*:3498–3505(1997).
33. Sato, K., S. Ueno, and J. Yano, Molecular Interactions and Kinetic Properties of Fats, *Prog. Lipid Res. 39*:91–116 (1999).
34. Bunjes, H., M.H.J. Koch, and K. Westesen, Influence of Emulsifiers on the Crystallization of Solid Lipid Nanoparticles, *J. Pharm. Sci. 92*:1509–1520 (2003).
35. Higami, M., S. Ueno, T. Segawa, K. Iwanami, and K. Sato, Simultaneous Synchrotron Radiation X-ray Diffraction–DSC Analysis of Melting and Crystallization Behavior of Trilauroylglycerol in Nanoparticles of Oil-in-Water Emulsion, *J. Am. Oil Chem. Soc. 80*:731–739 (2003).
36. Hamada, Y., I. Kobayashi, M. Nakajima, and K. Sato, Optical and Interfacial Tension Study of Crystallization of *n*-Alkane in Oil-in-Water Emulsion Using Monodispersed Droplets, *Cryst. Growth Design 2*:579–584 (2002).
37. Aquilano, D. and G. Squaldino, Fundamental Aspects of Equilibrium and Crystallization Kinetics, in *Crystallization Processes in Fats and Lipid Systems,* edited by N. Garti and K. Sato, Marcel Dekker, New York, 2001, pp. 1–51.
38. Ubbelohde, A.R., *The Molten State of Matter,* John Wiley & Sons, Chichester, United Kingdom, 1978, pp. 6–53.
39. Vanapalli, S.A., J. Palanuwech, and J. Coupland, Stability of Emulsions to Dispersed Phase Crystallization: Effect of Oil Type, Dispersed Phase Volume Fraction, and Cooling Rate, *Coll. Surf. A 204*:227–237 (2002).
40. Krog, N., and K. Larsson, Crystallization at Interfaces in Food Emulsions, *Fat Sci. Technol. 94*:55–57 (1992).

[Received April 22, 2003; accepted February 18, 2004]